Surface nano-mechanical properties of bio-modified reclaimed asphalt binder

Cavalli M. C. [a], Mazza E. [a, b], Zaumanis M. [a], Poulikakos L. D. [a*]

[a] *Empa, Road Engineering/Sealing Components, 8600 Dübendorf, Switzerland*

[b] *ETH Zurich, Institute for Mechanical Systems, 8092 Zürich, Switzerland*

* Corresponding author

Überlandstr. 129, 8600 Dübendorf

+41 58 765 4807

lily.poulikakos@empa.ch

This document is the accepted manuscript version of the following article:

Cavalli, M. C., Mazza, E., Zaumanis, M., & Poulikakos, L. D. (2021). Surface nanomechanical properties of bio-modified reclaimed asphalt binder. Road Materials and Pavement Design, 22(6), 1407-1423. https://doi.org/10.1080/14680629.2019.1691042

Abstract

In this work, three different bio-based rejuvenators were added to the reclaimed asphalt pavement (RAP) binder: a vegetable oil, a cashew nut shell oil and a tall oil. To better understand the microstructural morphology, atomic force microscopy (AFM) was used before and after aging. Quantitative nano-mechanical mapping (QNM) showed how the addition of rejuvenators had an effect on the surface elastic moduli of RAP. Changes of the microstructure in modified RAP binders as a function of aging treatments were seen. Generally, the microstructures show four domains topographically, while two distinct domains are present in the phase image. It has been observed that these two different domains correspond to zones with different mechanical properties. Comparison between the "bees" surface's elastic moduli and the bulk elastic moduli for a virgin bitumen showed that surface's moduli were consistently higher than the bulk moduli contributing to the formation of the "bee" structures. "Bees" were observed to be composed of periodic ripples with wavelength in the order of 400 for the aged virgin binder and 600 nm for the unaged one while amplitude equal to 8 and 15 nm for the aged and unaged case respectively. The results presented in this paper contribute to an improved understanding of the link between surface and bulk properties of bitumen.

Keywords: RAP; rejuvenators; AFM; elastic moduli; bee structures.

1. Introduction

Asphalt concrete is a material composed of mineral aggregates and bituminous binder. In order to decrease their environmental footprint, these materials are produced by substituting parts of the virgin components by recycling reclaimed asphalt pavement (RAP) (Cavalli et al., 2016). Mechanical properties of RAP binders have been thoroughly investigated in the past. In particular, a considerable amount of work has been done on the characterization of the aged binder contained in the RAP, through both mechanical and physico-chemical approaches (Cavalli, Zaumanis, Mazza, Partl, & Poulikakos, 2018). Specifically, it is known that the aging process affects the chemical and physical characteristics of bitumen thus modifying the original rheological properties (Cavalli et al., 2018). In order to restore the properties of the aged binders, it is common to add chemical products called "rejuvenators" into the RAP binder in order to restore the properties of the aged binder (Oliviero Rossi et al., 2015). The investigation of the bitumen's microstructure and how it is affected by rejuvenators can help our understanding of how these modifiers affect the material. It is widely accepted that bitumen consists of a colloidal suspension, (Nellensteyn & Roodenburg, 1933), where asphaltenes are dispersed in maltenes (Pfeiffer & Saal, 1940). Atomic force microscopy (AFM) can be applied to characterize binders' morphology. Previous researches have shown that the waxes in bitumen can appear in the form of a "bee"

structure (Das, Baaj, Tighe, & Kringos, 2016a). A detailed AFM microscopy study of bitumen samples under mechanical strain and under different sample preparation and storage conditions showed how "bee" structures are very thin (ca. 10 nm) with hills being harder than the valleys in terms of elastic modulus (Hung & Fini, 2015). In addition, it was observed how AFM imaging revealed relevant topological evolution of the bitumen with water exposure at elevated temperature (Hung, Goodwin, & Fini, 2017). Questions remain as to the origin, properties, and subsurface structure of these features as well as their relation to material performance. Several studies have analysed the surface properties of reclaimed asphalt binder after the addition of rejuvenators. For example addition of additives have caused a drastic change in the binder's morphology (Hung, Mousavi, Pahlavan, & Fini, 2017).
The temperature effect on morphology of asphalt binder modified with polymers was studied in (Navarro, Partal, García-Morales, Martinez-Boza, & Gallegos, 2007) where it was shown how the polymer addition leads to "bee"-shaped micro-structure regions with lower thermal susceptibility.
In recycled binder mixture, AFM has been used to study the rejuvenation process before and after aging (Menapace et al., 2018). Bio-based rejuvenators have been promising for revealing how bio-oil mitigates the number of "bee" structure in the binder's surface. This could be an indication how rejuvenators are effectively able to enhance the diffusion of certain asphalt compounds (Ali, Mehta, Nolan, Purdy, & Bennert, 2016). In (Rashid, Hossain, & Bhasin, 2019) the microstructures as well as the nanomechanistic properties of the blended binders were found significantly different from those of the base binder; the elastic modulus of 60% RAP was over 70% higher than that of the base binder. The modulus was found to be correlated with the morphology. However, the nanoscale properties were in agreement with microscale properties of the tested binders.
The aim of this work is to better understand the changes of the microstructures in RAP binder after the addition of rejuvenators before and after aging. In addition, AFM was used as a tool to measure the surface's elastic moduli for all the binder before and after aging. A comparison between the "bees" surface's elastic moduli and the bulk elastic moduli for a virgin bitumen has been proposed as well.

2. Materials and Methods

The bituminous binder from RAP was extracted using toluene as solvent. The binder content was 4.60% by weight of the mixture (EN 12697-1). The extracted RAP's binder had a penetration of 22×10^{-1} mm at 25° C (EN 1426) and a softening point equal to 65.7° C (EN 1427). 50/70 virgin binder used in this study showed a penetration of 62 x 10^{-1} mm at 25° C and a softening point of 48.75° C. Three commercial bio-based rejuvenators were used: rejuvenator "A" from natural seed oil, rejuvenator "B" from cashew nut shell oil and rejuvenator "C" from tall based oil. The rejuvenator dosage was set at 5% by mass of RAP binder following a previous work by authors (Cavalli et al., 2018).

2.1 Rejuvenation Procedure

100 g. of RAP binder were placed in an oven for 20 minutes at a temperature equal to the softening point, plus 80° C (EN 12697-1). The amount of time was found to be the minimum for the RAP binder to become liquid. Rejuvenators (which were at room temperature) were added to the hot binder and were placed in the Speed Mixer™ for one minute at 3500 rpm (total mass of this binder mixture was 105 g). One minute was visually found suitable for homogenization. Thereafter the rejuvenated binders were laboratory aged using Rolling Thin Film Oven Test (RTFOT) ("EUROPEAN STANDARD EN 12607-1: Bitumen and bituminous binders — Determination of the resistance to hardening under the influence of heat and air —," 2007) and subsequently Pressure Aging Vessel (PAV) ("EUROPEAN STANDARD 14769:2012: Bitumen and bituminous binders - Accelerated long-term ageing conditioning by a Pressure Ageing Vessel (PAV)," 2012). The combined aging procedures are expected to simulate both early stage aging and in situ aging (Mousavi, Pahlavan, Oldham, Hosseinnezhad, & Fini, 2016).

2.2 Topography and phase imaging

Annealing is important to enable the micro-structure of the asphalt binder to return to its original form and eliminate any artefacts that may be attributable to the solvent cast spin-coating process. However, in (Pauli, Grimes, Beemer, Turner, & Branthaver, 2011) it was shown how the nanometre range sample can have a direct impact on the AFM images, as the size and shape of the micro-structures change significantly with the relative film thickness. In addition, steric hardening effects the sample in the spin-casting procedure and can also alter the bitumen microstructure (Pauli et al., 2011). In the heat casting method, the asphalt binder needs to be mixed properly by stirring around 120 ± 10°C (depending on the types of binder) to avoid biases due to samples' inhomogeneity (Das, Baaj, Tighe, & Kringos, 2016b). A sample holder can be used to place approximately 20–30 mg of hot liquid binder and keeping it on a hot plate for 5 min at the same temperature. This will allow the binder to spread out by creating a smooth surface. Afterwards, the specimens need to be left horizontally and be covered to prevent dust pick up for at least 24 h at 25°C prior to test. Since all specimens generally go through the same preparation process, it can be assumed that oxidation during sample preparation can be ignored or is at least constant amongst all specimens (Das, Kringos, Wallqvist, & Birgisson, 2013). Thus, authors followed the preparation method as prescribed in (Soenen et al., 2014), so that 15 mg of binder was buttered and placed on a glass slide. The glass slide was covered to prevent dust accumulation with a glass plate and subsequently placed in a ventilated oven at 110° C for 20 minutes. Afterwards, the covered sample was left to cool for 24 hours prior to testing in a humidity controlled chamber. Subsequently, AFM measurements were performed at room temperature. Asphalt binders' surface was analysed using an Icon3 AFM device from Bruker. The data were collected using Nanoscope 8.15. The conical tip, consisted of a silicon probe, type RTESPA-150 from Bruker with a resonant frequency of 150 kHz and spring constant of 6 N/m, a cantilever length equal to 125 μm and

width of 35 µm and a tip radius equal to 8 nm. The scan size was equal to 10 µm x 10 µm with a scan rate of 0.5 Hz.

2.3 Force mapping

The AFM force mapping was also performed on a Bruker Icon3 AFM in PeakForce Quantitative Nanomechanical property Mapping (QNM) mode with a Nanoscope V controller. The resulting force curves were evaluated using Nanoscope 8.15 software. The AFM QNM scans were performed on bitumen at room temperature and under humidity-controlled condition (RH = 40% and T =23° C). The sample's preparation and cantilever probe followed what was described in the previous section for topography imaging. The spring constant was determined by the thermal tune method (Hutter & Bechhoefer, 1993). To perform quantitative measurements, it was necessary to calibrate the cantilever in order to identify the point of contact and then measure the precise probe geometry and the cantilever spring constant. RTESPA-150 was found to be the suitable probe for QNM measurements of bitumen. In addition, the tip radius was calibrated using Bruker PDMS-12 sample with nominal elastic modulus of 3.5 MPa. QNM mode measurements were performed as follows: the probe was oscillated in the z-direction at 2 kHz at the same time the sample was scanned line by line at a rate of 1 Hz. Every image was built up of 512 per 512 pixels each originating from force curve evaluation. To obtain the elastic modulus E* at the sample surface, in QNM mode, the retraction curve was then fitted by a specific software by using the Derjaguin–Muller–Toporov (DMT) model (Derjaguin, Muller, & Toporov, 1975).

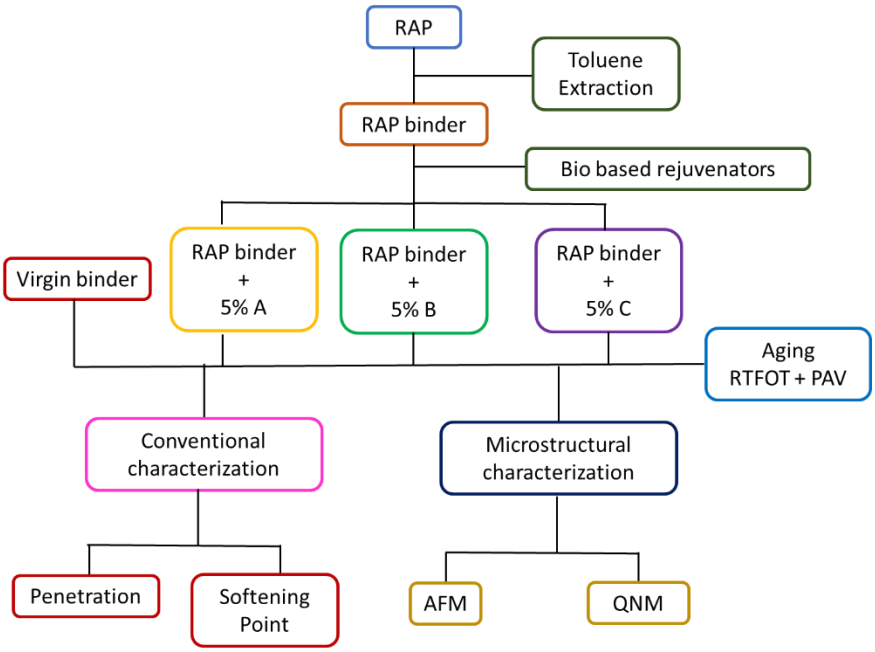

Figure 1 Flow chart of the research work.

3. Results and Discussion

3.1 AFM topography imaging

Microstructures of the 50/70 virgin bitumen can be seen in Figure 2. While the topography shows the surface height morphology, the phase image provides qualitative indication of different mechanical properties among diverse domains as a result of variations of cantilever's oscillation due to interaction between the bitumen's surface and the AFM probe. Those interactions cause a change in the cantilver's resonant frequency resulting in a phase's lag which is indicated by the phase angle variations reported in the corresponding images. Phase mapping can provide indication on variations in terms of viscoelasticity along the surface (Menapace et al., 2018).

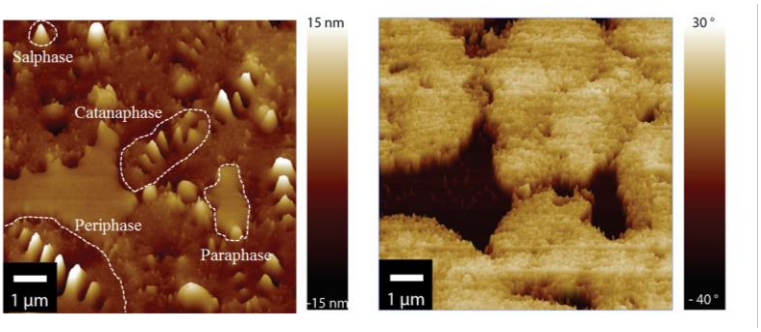

Figure 2 AFM height morphology image of the virgin binder 50/70 (left) and phase visualization (right) (3D visualization of image size 10 x 10 µm).

The microstructure of bituminous binder, showing the presence of the so called "bee" structures, has been investigated since their first discovery (Loeber, Sutton, Morel, Valleton, & Muller, 1996). "Bee" structures have been attributed to the interaction between paraffinic waxes and the remaining non-wax asphalt components (Pauli et al., 2011). Figure 2 shows how virgin asphalt binder is not a homogenous material but contains four distinct domains. The four different zones depicted in **Error! Reference source not found.** are: catanaphase ("bee" shaped), periphase (around the catana shape), paraphase (matrix phase) and salphase which are phase spots and linked to the presence of non-dispersed compounds in the matrix. Wrinkling domains containing the "bee" structures (with major and minor axes of a few microns) dominate the surface of the virgin binder.

To further investigate the "bee" formation, in this research AFM imaging was carried out on the extracted RAP binder itself. As it is possible to see from Figure 3, there is a uniform matrix with few salphases appearing in the phase image. Since RAP was obtained after toluene extraction, the presence of this solvent could influence the morphology. However, in a previous work by same authors (Cavalli, Partl, & Poulikakos, 2017), a bituminous binder was immersed in toluene and AFM had been performed after the total evaporation of the solvent. The microstructure observed presented the same morphology as before immersion in toluene.

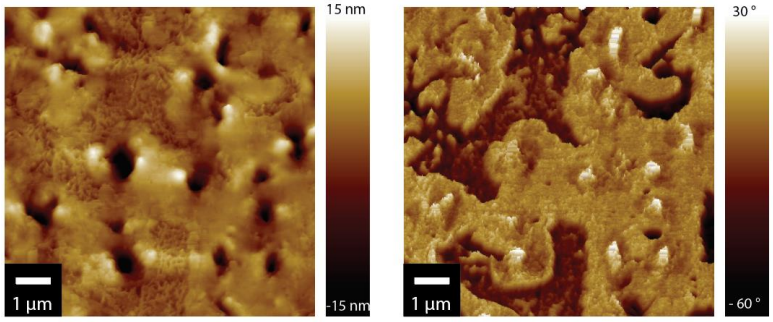

Figure 3 AFM height morphology image of the RAP binder with 20.3% asphaltenes (left) and its phase visualization (right) (10x10 µm).

As further step, rejuvenators were added to the RAP binder. As shown in Figure 4, the addition of rejuvenators affected the morphology of the RAP binder showing the formation of new structures which have different topography and phase images. In Figure 3 a) and b), the matrix phase was not homogenous presenting new branch formations which could be caused by the nucleation of waxes (Chen, Zhao, Zhang, & Wang, 2007). On the contrary, Figure 3 c) and d) showed several salphases with hills and valleys. Images of the RAP + 5% C, displays evidences of several branch and ramifications similar to RAP + 5% A as shown in Figure 3 e) and f).

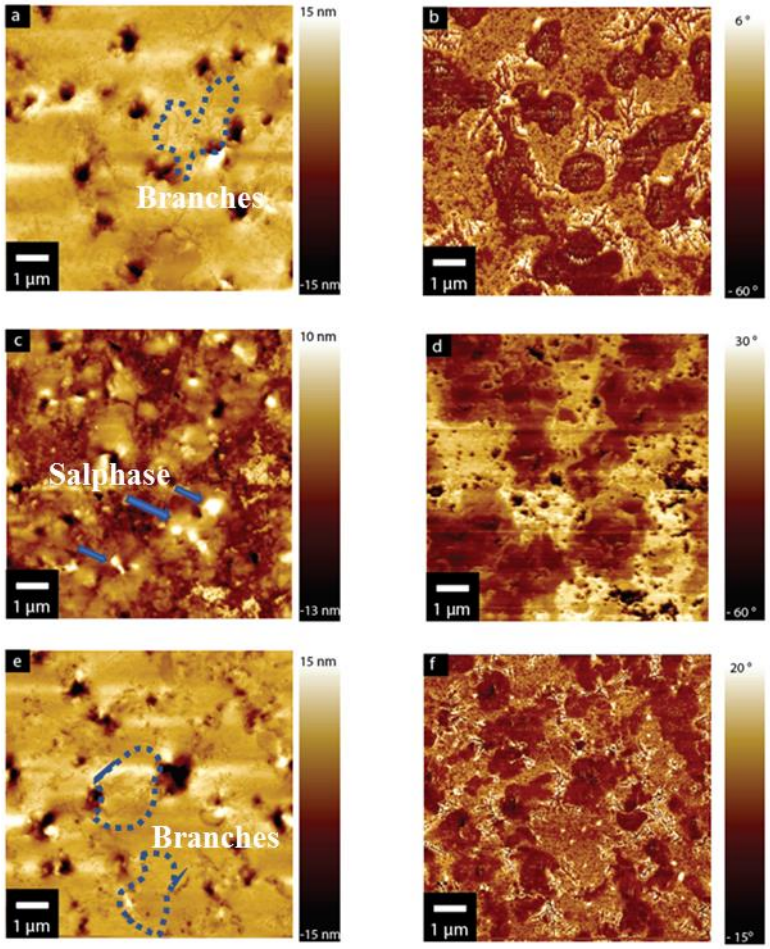

Figure 4 AFM height morphology image (10x10 µm) of the RAP plus 5% A (a) and corresponding phase image (b); RAP plus 5% B (c) and its phase image (d); and RAP plus 5% C (e) and its phase image (f). Branches are indicated with a dotted line while salphases are outlined with arrows.

As shown in Figure 5, by comparing the AFM images of the aged RAP binder and the aged virgin bitumen, it can be stated that aging can affect the morphology of both virgin binder and RAP binder. Aged virgin binder, represented in Figure 4 a), displays "bee" structures with homogenous paraphases and less periphases, whereas the RAP binder, Figure 4 b), and rejuvenated RAP binder do not show any "bee" structures. Aged RAP + 5% A and aged RAP + 5% C display similar morphologies. By increasing the content of asphaltenes, as in the aged RAP binder, salphases (resulting in the phase image as white spots) are more visible than before aging (Figure 4). This could be an indication that aging the RAP binder could cause a phase separation between the fractions observed in the RAP binder morphology. Aged RAP + 5% A and aged RAP + 5% C show the formation of branches as shown in Figure 5 c) and e). Hills and valleys are visible in all the three modified RAP binder.

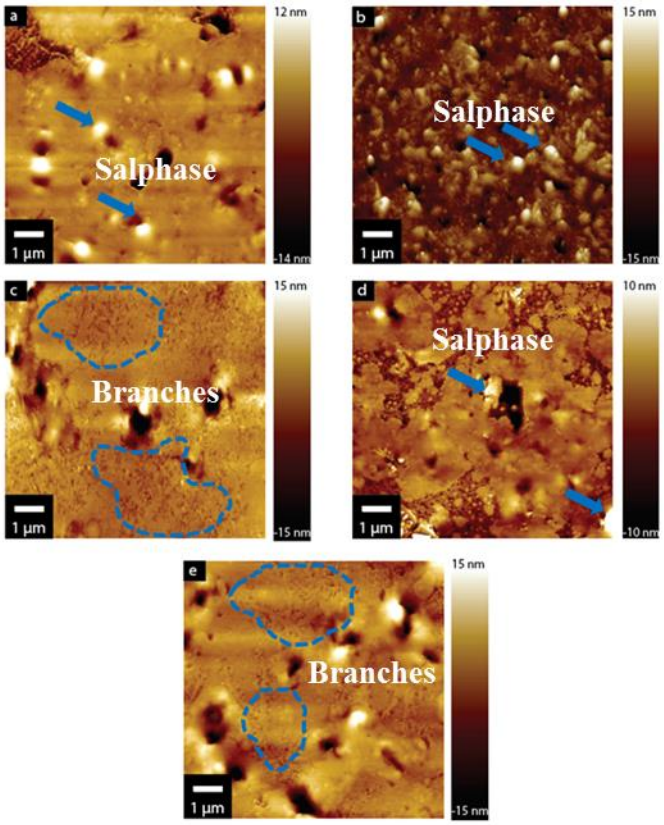

Figure 5 AFM topography images of the different rejuvenated RAP binder after RTFOT/PAV aging (size 10 x 10 µm). From top left to bottom (clockwise): a) Aged virgin bitumen 50/70; b) Aged RAP binder; c) Aged RAP + 5% A; d) Aged RAP + 5% B and e) Aged RAP + 5% C. Branches are indicated with a dotted line while salphases are outlined with arrows.

3.2 Qualitative analysis of phase images

As can be seen in Figure 6, in order to gain qualitative information, phase images of each binder were converted to 8-bit grey scale to distinguish the two primary domains in bitumen phase images. By using this methodology, each pixel was assigned a colour value between 0 (black) and 255 (white) within the grey scale as shown in Figure 6. This procedure creates a statistical distribution of the number of pixels depending on their colour intensity. Although phase scale are not numerically the same for each image, the shape of the Gaussian curve obtained from the histograms has been observed to be similar for all the images studied (two different Gaussian curves with two maxima). The Gaussian curves were considered for the characterization of each 8-bit image so that the algorithm was not influenced by the quantitative numerical values of the phase slag. The algorithm applied for the conversion was the same for each image with each RGB image converted in greyscale by linearly scaling (Schindelin et al., 2012).

In the end by applying a threshold, a black and white image was obtained as can be seen in the sample used in Figure 6..

The black and white binary image was afterwards used to calculate the area corresponding to the white area and the area belonging to the black zones representing the two domains present in bitumen. These operations were repeated for four images per binder. The method was developed by using ImageJ/Fiji software (Schindelin et al., 2012). No further data processing such as noise smoothing was performed.

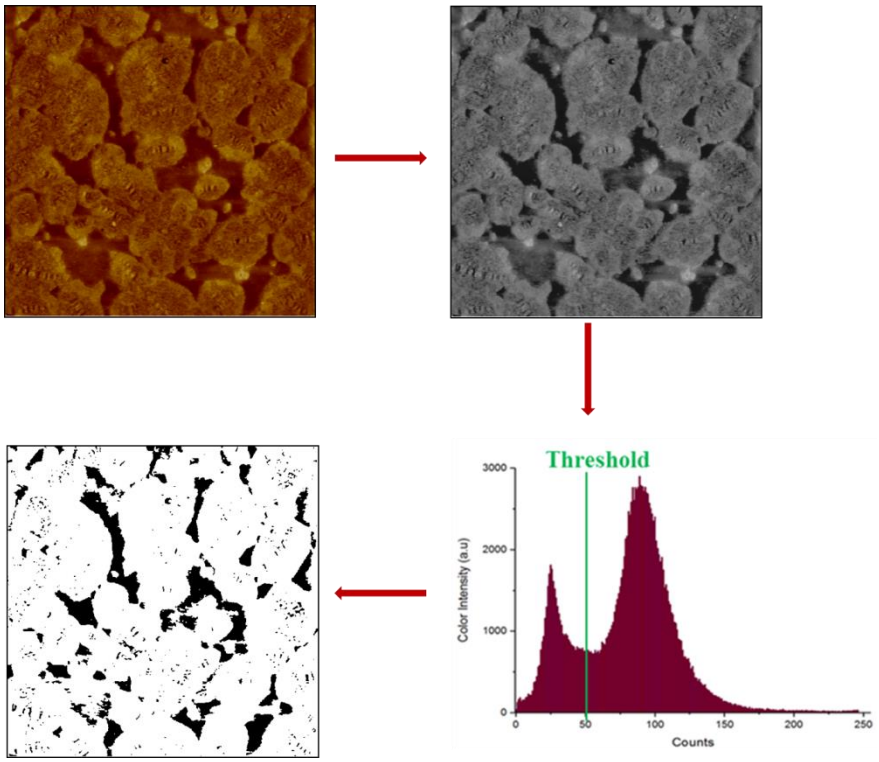

Figure 6 Steps for the application of the threshold procedure.

In the resulting binary images white areas represent the catana plus peri phase and dark areas represent the paraphrase. As can be seen in Figure 7, RAP presented higher whiter zones compared to other binders. The general trend is that aging caused a change in the proportion of whiter/ darker areas together with an increase of white and decrease of darker areas. The standard deviation was calculated over four different images.

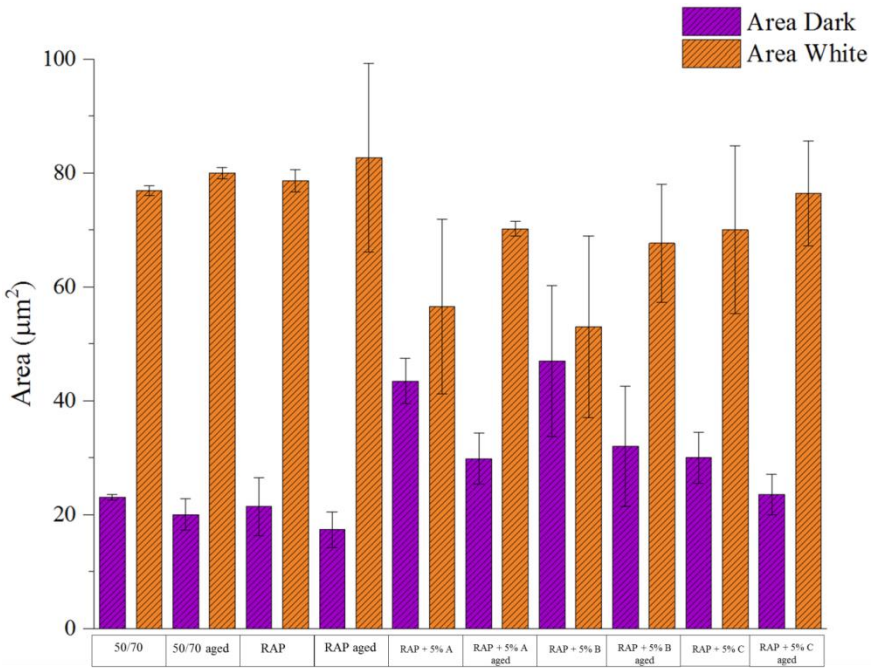

Figure 7 Area dark and area white for each binder and its standard deviation.

In addition, the ratio between the dark and the white area for each binder was compared with the complex shear modulus G* obtained by rheological measurement in own previous investigation (Cavalli et al., 2018). The G* indicated in Figure 8 was obtained at 20° C under quasi-static conditions. These values were chosen in order to have a direct comparison with the sample condition during AFM measurements (room temperature equal to 22° C). In Figure 8, a general trend can be seen: aging causes a lower ratio of dark/white and an increase in complex moduli. The plot presented shows that there is a qualitative link between the images showing the cantilever phase slag as a result of interaction with the surface of the material and the bulk properties in terms of complex moduli. These results show a clear relationship between bulk and surface properties.

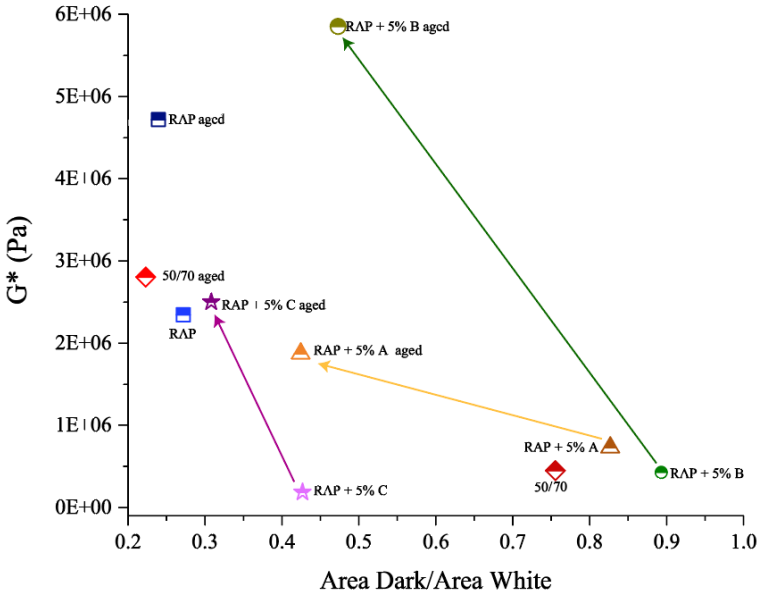

Figure 8 G* and ratio between the dark are and the white area for each binder.

3.3 Quantitative nano-mechanical mapping

As can be seen in Figure 9, the virgin binder images present a softer paraphase surrounding the "bee" structures. On the contrary, RAP binder images appear generally brighter with fewer softer spots. The following general observation can be made: RAP binder elastic moduli at the surface are on average higher than the virgin binder both at unaged and aged state. As can be seen in Figure 9, after aging the elastic moduli for both RAP binder and virgin binder increases. In particular, in Figure 11 a) and c) it's possible to observe how after aging, "bees" appear to become smaller and gain higher elastic moduli. In Figure 9 b) and c), it is shown how the morphology of RAP binder does not change significantly after aging however, the elastic modulus increases by around 46%.

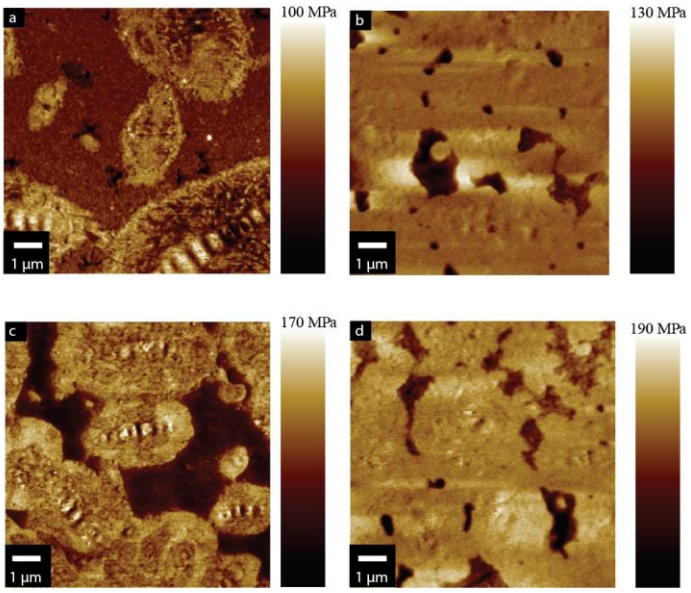

Figure 9 AFM QNM images (10 x 10 µm). a) Virgin binder 50/70 unaged; b) RAP binder unaged; c) Virgin binder 50/70 aged; d) RAP binder aged.

As shown in Figure 10, RAP plus 5% A and RAP plus 5% C show the same branch formations discussed in the previous section using tapping mode, both in unaged and aged states. Although the origin of these branch formations is not clear, QNM mode demonstrates how these branch formations are softer than the matrix in terms of elastic moduli. In general, all the rejuvenated binders in the unaged state, show lower elastic moduli (at unaged stage from 80 MPa to 95 MPa) than the RAP binder (130 MPa). This can be an indication of the softening potential of rejuvenators in reducing moduli at the surface of the RAP binder. As shown in Figure 10, RAP plus 5% B presents topography that is similar to the RAP binder (Figure 11) with higher elastic moduli (105 MPa) than the other two modified binders (80 and 95 MPa). As demonstrated in Figure 10 from d) to f), all binders increase their elastic moduli in the surface after laboratory aging. In particular, RAP plus 5% B was affected more by aging than the other two binders.

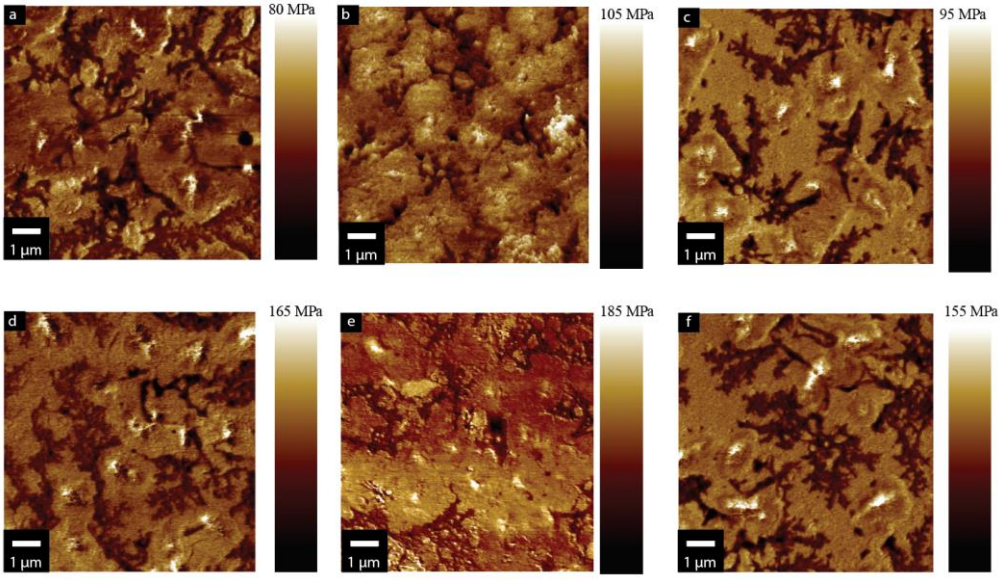

Figure 10 AFM QNM images (10 x 10 µm). From top clockwise: a) RAP + 5% A b) RAP + 5% B c) RAP + 5% C d) RAP + 5% A aged e) RAP + 5% B aged f) RAP + 5% C aged.

The data obtained with QNM measurements were used to create Gaussian functions describing the distribution of the elastic moduli as average of five different images. In addition, cumulative distribution functions for each binder were calculated. As can be observed in Figure 11, at unaged stage, the RAP binder presented a broader range of elastic moduli compared to the other binders. RAP binder elastic moduli were overall higher while RAP + 5% B and virgin binder 50/70 had a similar trend. At unaged stage, RAP + 5% B and RAP + 5% C were able to restore the RAP binder moduli. After aging,

Gaussian curves become broader and there's a general shift of the curves towards higher elastic moduli. Generally despite aging, RAP + 5% A and RAP + 5% C showed lower elastic moduli than all the other binders. Furthermore comparing the unaged and aged states of the binders show that the RAP + 5% C had lower aging susceptibility (peak Modulus equal to 95 MPa at unaged stage and 155 MPa at aged stage). However, in general it can be observed how each rejuvenated RAP increases its elastic modulus after aging. Instead, the RAP binder peak modulus increases from 120 MPa (unaged stage) to 180 MPa.

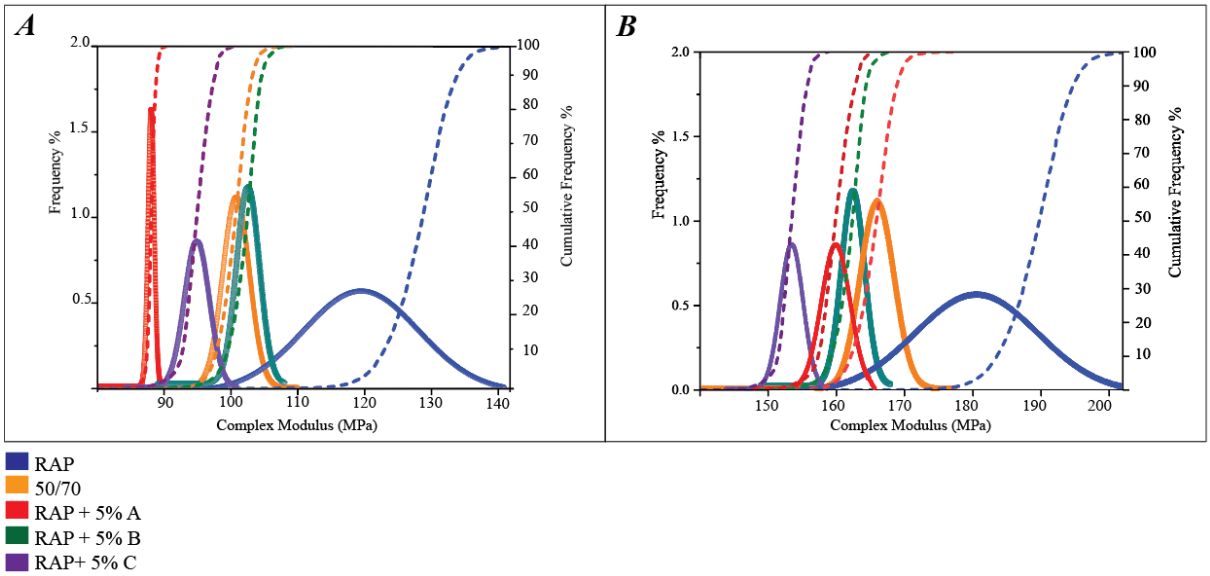

Figure 11 Gaussian distribution and cumulative frequency curve for unaged binders (A) aged binders (B). Data were obtained as average of five images per binder.

Similar results were obtained by analysing the 50th percentile values of elastic moduli at the surface with the QNM method. As can be seen in Figure 12, before aging, all rejuvenated binders showed lower elastic moduli. After aging, the elastic moduli at the bulk increased for all binders. However, it can be noticed how as a general trend, the elastic moduli of all rejuvenated binders appeared lower than that of the neat RAP. It is important to outline that this trend was confirmed by rheological measurements at the bulk, as shown by Cavalli et al. (Cavalli et al., 2018). Thus, aging has a prominent effect both at the bulk and at the surface. In addition, the effect of rejuvenators in restoring the mechanical properties of the reclaimed binder at the bulk, were confirmed by measurements of the elastic modulus at the surface. Bitumen being a viscoelastic material has properties that are temperature and frequency dependent. As described in (Cavalli et al., 2018) for all frequency ranges, RAP + 5% A and RAP + 5% C had similar complex moduli after aging.

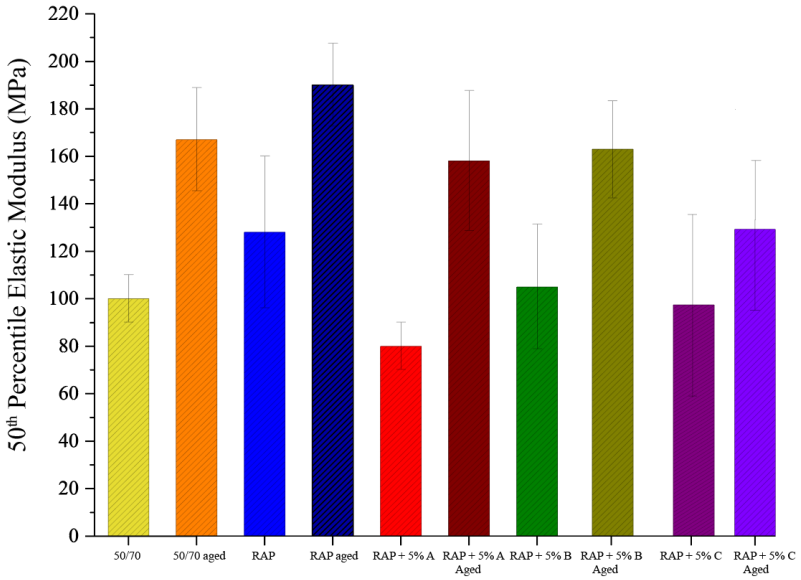

Figure 12 50th percentile elastic modulus for all binders with standard deviation calculated as average of five measurements.

QNM uses linear elastic contact mechanics models to interpret results obtained for viscoelastic materials like bitumen. Thus, the present findings have to be considered as indicative of the modulus values for the specific deformation rate applied in the measurement. Moreover, what was measured with QNM was two orders of magnitude higher than the bulk, i.e. complex moduli results at quasi static conditions for 20° C were in the range 0.45-2.42 MPa while at the surface, the 50th percentile elastic moduli presented a range between 100 and 190 MPa. This indicates that bulk properties are different from surface properties. In line with this conclusion, the formation of "bees, as shown in Figure 2, is a consequence of the presence of a stiff and thin surface layer. This effect is quantitatively analysed in the next section.

3.4 Comparison of the bulk and surface properties of the "bees" structures

As can be seen in Figure 13, virgin binder 50/70 presents wrinkled surface structures known as "bee" structures presenting undulated patterns which are not perfectly regular. The pattern can be represented, in a first approximation, as sinusoidal wrinkles characterized by a certain wavelength λ_o and a maximum amplitude $2A_0$.

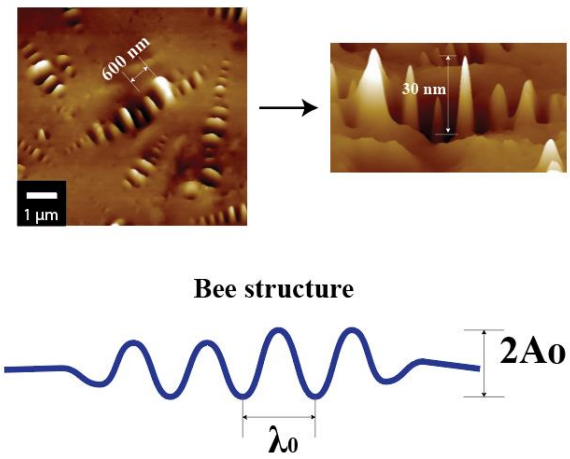

Figure 13 Top part: AFM topography image of the virgin binder 50/70 with corresponding measurement of wavelength λ_o and maximal amplitude $2A_o$ of the "bee" structure. Bottom part: representation of the "bee" structure with corresponding wavelength λ_o and the maximum amplitude $2A_o$.

Jäger et al. (Jäger, Lackner, Eisenmenger-Sittner, & Blab, 2004) were the first ones to investigate the relative stiffness of different phases in asphalt binder. It was observed how the micro-structure and its surrounding matrix showed different relative stiffness. Many studies have been performed in the past to understand the origin of the "bees" formation. The most widely accepted hypothesis is that the "bees" are wrinkled film of crystallized paraffin (Lyne, Wallqvist, & Birgisson, 2013) generated through the difference in the contraction rate of the film and the underlying material. It has been observed that stiff laminated films on viscoelastic substrates might lead to the formation of wrinkled structures on the surface (Jiang et al., 2007). The research by Hung & Fini (Hung & Fini, 2015) showed the validity of this assumption for a bitumen presenting "bees".

As depicted in Figure 13, the values of A_0 and λ_o characterize the "bees" geometry. For the case studied, as average among five "bees", the maximum A_0 was found to be equal to 15 nm with a wavelength λ_o equal to 600 nm for the unaged virgin binder. For the aged virgin binder, A_0 and λ_o were measured as 8 nm and 400 nm respectively. These values are in agreement with average "bees" dimensions as reported in previous works (Hung & Fini, 2015).

Based on [30], the model representing "bees" formation considers the plain strain elastic moduli $\bar{E}_{film}$ and $\bar{E}_{substrate}$ defined as follows:

$$\bar{E} = E^*/(1-\upsilon^2) \quad (1)$$

where E^* is the magnitude of the complex elastic modulus and υ is the Poisson's ratio.

In order to obtain $\bar{E}_{substrate}$, it is necessary to convert the complex shear modulus G* values measured in (Cavalli et al., 2018) into its corresponding E^* values. G* values were obtained for quasi static loading at room temperature by using the dynamic shear rheometer, DSR (Cavalli et al., 2018), and for these conditions virgin bitumen has generally a Poisson's ratio equal to 0.40 (Di Benedetto, Delaporte, & Sauzéat, 2007). It is hereby assumed that the same value of Poisson's ratio can be used for both film and substrate. E^* can thus be calculated as:

$$E^* = 2G^*(1+\nu) \quad (2)$$

The substitution of E^* into Equation (2) provides $\bar{E}_{substrate}$. $\bar{E}_{film}$ is obtained by inserting in Equation (2) the corresponding 50th percentile elastic moduli as reported in Figure 12. Results are summarized in Table 1.

Table 1 Results obtained from the rheological measurements (Cavalli et al., 2018) with corresponding elastic modulus as well elastic modulus obtained after AFM QNM.

Material	G* (MPa)	E* (MPa)	$\bar{E}_{substrate}$ (MPa)	$\bar{E}_{film}$ (MPa)	$\frac{\bar{E}_{film}}{\bar{E}_{substrate}}$
50/70 unaged	0.44	1.23	1.46	119.04	81
50/70 aged	2.43	6.80	8.10	202.38	25
RAP unaged	2.34	6.55	7.80	154.76	20
RAP aged	5.16	14.44	17.2	226.19	13

Generally, the model for "bees" formation (Jiang et al., 2007) requires that the film is significantly stiffer than the substrate ($\bar{E}_{film} > \bar{E}_{substrate}$). Hung & Fini (Hung & Fini, 2015) used properties from the literature and estimated the ratio $\frac{\bar{E}_{film}}{\bar{E}_{substrate}}$ for bitumen to be in the order of magnitude of 100. As reported in Table 1, the ratio was about 81 and 25 for the unaged and aged virgin binder respectively, where "bees" formation was observed. This ratio was considerably lower with 20 and 13, for the unaged and aged RAP respectively. Thus, these results might rationalize the fact that no "bee" structures have formed on the surface of the RAP binder. The formation of the stiff surface layer might be associated with the cooling conditions of the sample (Hung & Fini, 2015). This process was not specifically analysed for the present samples, but no systematic differences are expected between virgin and RAP binders.

The amplitude and wavelength of the wrinkled domains predicted based on the model in (Jiang et al., 2007) are in line with the ones measured for the present "bees", providing a confirmation of the model validity. A difference in the "bees" size before and after aging has been observed, with reduced

amplitude an wavelength. In particular, the wavelength reduced from 600 to 400 nm, i.e. by a factor of 1.5. Based on the model in (Jiang et al., 2007), the wavelength scales with the power 1/3 of the moduli ratio, which leads in this case to a factor 1.47 between the two material, in excellent agreement with experimental observations. Furthermore, the model predicts that the critical contraction strain to form "bees" is by about 15% and 50% larger than the one of the aged 50/70 binder, due to their lower moduli ratios. This might explain the absence of wrinkles for the RAP samples.

4. Conclusions

Atomic force microscopy (AFM) has been utilized to study the topography and phases of different binders: a virgin binder 50/70, a RAP binder and three different bio-modified binders. Each material was analysed before and after laboratory aging. The main findings from the AFM studies are as follows:

i. RAP binder and virgin binder display significantly different microstructures; the four domains observed in the virgin binder, including "bee" structures, do not form in RAP binder microstructure.

ii. Aging affects the morphology of both virgin binder and RAP binder

iii. Generally, the microstructures show four domains topographically, while two distinct domains are present in the phase image. It has been observed that these two different domains correspond to zones with different mechanical properties.

iv. In the topography images, aging caused a reduction of periphase which was associated to the softer part of the microstructure.

v. The addition of two types of rejuvenators (A and C) created new branches at the surface of the RAP binder with lower moduli.

vi. A correlation between phase images (qualitative mechanical properties) and rheological measurements have been proposed.

vii. Quantitative nano-mechanical mapping of elastic moduli along samples' surface was possible. Generally, surface's elastic moduli ranged from 80 MPa up to 200 MPa.

viii. In general, RAP binder surface was stiffer than the other binders. The addition of rejuvenators decreased the elastic moduli of the RAP binder. As a result of aging, the surface elastic moduli of all binder increased.

ix. Using the Gaussian distribution of the surface moduli it was shown how rejuvenators from natural seed oil and from tall oil showed less aging susceptibility.

x. "Bees" were observed to be composed of periodic ripples with wavelength in the order of 400 for the aged virgin binder and 600 nm for the unaged one while amplitude equal to 8 and 15 nm for the aged and unaged case respectively.

xi. Surface modulus was consistently higher than the bulk modulus contributing to the formation of the "bee" structures for the virgin binder.

In conclusion, the addition of rejuvenators results in the formation of new structures on the surface of the RAP binder. This work correlates nano-mechanical properties at the surface with the bulk properties of modified asphalt binders. It was found that a common trend between the materials mechanical properties before and after aging exist for both bulk and surface properties. In particular, it has been demonstrated how rejuvenators could soften the RAP's binder both at the bulk and at the surface.

Acknowledgments

The authors would like to thank the Swiss federal office for the environment grant number UTF 489.19.14 / IDM 2006.2423.487 for the financial support of this project. Authors would like to greatly acknowledge Prof. Dr. Manfred Partl for his inputs in this research. Dr. Ulrich Müller from the Nanoscale Materials Science Laboratory at Empa for the technical support and the overall discussions, Dr. Michele Griffa from the Concrete/Construction Laboratory at Empa for the support in the imaging analysis and Professor Nancy Burnham from Worchester Polytechnic Institute for the fruitful discussions.

References

Ali, A. W., Mehta, Y. A., Nolan, A., Purdy, C., & Bennert, T. (2016). Investigation of the impacts of aging and RAP percentages on effectiveness of asphalt binder rejuvenators. *Construction and Building Materials*, *110*, 211–217. https://doi.org/10.1016/j.conbuildmat.2016.02.013

Cavalli, M. C., Griffa, M., Bressi, S., Partl, M. N., Tebaldi, G., & Poulikakos, L. D. (2016). Multiscale imaging and characterization of the effect of mixing temperature on asphalt concrete containing recycled components. *Journal of Microscopy*, *264*(1), 22–33. https://doi.org/10.1111/jmi.12412

Cavalli, M. C., Partl, M. N., & Poulikakos, L. D. (2017). Effect of aging on the microstructure of reclaimed asphalt binder with bio-based rejuvenators. In *4th International Symposium on Asphalt Pavement & Environment*.

Cavalli, M. C., Zaumanis, M., Mazza, E., Partl, M. N., & Poulikakos, L. D. (2018). Effect of ageing on the mechanical and chemical properties of binder from RAP treated with bio-based rejuvenators. *Composites Part B: Engineering*, *141*, 174–181. https://doi.org/10.1016/j.compositesb.2017.12.060

Chen, W., Zhao, Z., Zhang, X., & Wang, L. (2007). Thermodynamic phase equilibria of wax

precipitation in crude oils. *Fluid Phase Equilibria*, *255*(1), 31–36. https://doi.org/10.1016/j.fluid.2007.03.015

Das, P. K., Baaj, H., Tighe, S., & Kringos, N. (2016a). Atomic force microscopy to investigate asphalt binders: a state-of-the-art review. *Road Materials and Pavement Design*, *17*(3), 693–718. https://doi.org/10.1080/14680629.2015.1114012

Das, P. K., Baaj, H., Tighe, S., & Kringos, N. (2016b). Atomic force microscopy to investigate asphalt binders: a state-of-the-art review Atomic force microscopy to investigate asphalt binders: a state-of-the-art review. *Road Materials and Pavement Design*, *17*(3), 693–718. https://doi.org/10.1080/14680629.2015.1114012

Das, P. K., Kringos, N., Wallqvist, V., & Birgisson, B. (2013). Micromechanical investigation of phase separation in bitumen by combining atomic force microscopy with differential scanning calorimetry results. *Road Materials and Pavement Design*, *14*, 25–37. https://doi.org/10.1080/14680629.2013.774744

Derjaguin, B., Muller, V., & Toporov, Y. (1975). Effect of contact deformations on the adhesion of particles. *Journal of Colloid And Interface Science*, *53*(2), 314–326. https://doi.org/10.1016/0021-9797(75)90018-1

Di Benedetto, H., Delaporte, B., & Sauzéat, C. (2007). Three-Dimensional Linear Behavior of Bituminous Materials: Experiments and Modeling. *International Journal of Geomechanics*, *7*(2), 149–157. https://doi.org/10.1061/(ASCE)1532-3641(2007)7:2(149)

EUROPEAN STANDARD 12697-1 Bituminous mixtures - Test methods for hot mix asphalt - Part 1: Soluble binder content. (2012).

EUROPEAN STANDARD 14769:2012: Bitumen and bituminous binders - Accelerated long-term ageing conditioning by a Pressure Ageing Vessel (PAV). (2012), 16.

EUROPEAN STANDARD EN 12607-1: Bitumen and bituminous binders — Determination of the resistance to hardening under the influence of heat and air —. (2007), *3*, 1–15.

EUROPEAN STANDARD EN 1426: Determination of the needle penetration. (2012).

EUROPEAN STANDARD EN 1427: Determination of the softening point-Ring and Ball method. (2012).

Hung, A. M., & Fini, E. H. (2015). AFM study of asphalt binder “bee” structures: origin, mechanical fracture, topological evolution, and experimental artifacts. *RSC Advances*, *5*(117), 96972–96982. https://doi.org/10.1039/C5RA13982A

Hung, A. M., Goodwin, A., & Fini, E. H. (2017). Effects of water exposure on bitumen surface microstructure. *Construction and Building Materials*, *135*, 682–688. https://doi.org/10.1016/j.conbuildmat.2017.01.002

Hung, A. M., Mousavi, M., Pahlavan, F., & Fini, E. H. (2017). Intermolecular Interactions of Isolated

Bio-Oil Compounds and Their Effect on Bitumen Interfaces. *ACS Sustainable Chemistry & Engineering*, *5*(9), 7920–7931. https://doi.org/10.1021/acssuschemeng.7b01462

Hutter, J. L., & Bechhoefer, J. (1993). Calibration of atomic-force microscope tips. *Review of Scientific Instruments*, *64*(7), 1868–1873. https://doi.org/10.1063/1.1143970

Jäger, A., Lackner, R., Eisenmenger-Sittner, C., & Blab, R. (2004). Identification of four material phases in bitumen by atomic force microscopy. *Road Materials and Pavement Design*, *5*(sup1), 9–24. https://doi.org/10.1080/14680629.2004.9689985

Jiang, H., Khang, D.-Y., Song, J., Sun, Y., Huang, Y., & Rogers, J. A. (2007). Finite deformation mechanics in buckled thin films on compliant supports. *Proceedings of the National Academy of Sciences*, *104*(40), 15607–15612. https://doi.org/10.1073/pnas.0702927104

Loeber, L., Sutton, O., Morel, J., Valleton, J.-M., & Muller, G. (1996). New direct observations of asphalts and asphalt binders by scanning electron microscopy and atomic force microscopy. *Journal of Microscopy*, *182*(1), 32–39. https://doi.org/10.1046/j.1365-2818.1996.134416.x

Lyne, Å. L., Wallqvist, V., & Birgisson, B. (2013). Adhesive surface characteristics of bitumen binders investigated by Atomic Force Microscopy. *Fuel*, *113*, 248–256. https://doi.org/10.1016/j.fuel.2013.05.042

Menapace, I., Garcia Cucalon, L., Kaseer, F., Arámbula-Mercado, E., Epps Martin, A., Masad, E., … King, G. (2018). Effect of recycling agents in recycled asphalt binders observed with microstructural and rheological tests. *Construction and Building Materials*, *158*, 61–74. https://doi.org/10.1016/J.CONBUILDMAT.2017.10.017

Mousavi, M., Pahlavan, F., Oldham, D., Hosseinnezhad, S., & Fini, E. H. (2016). Multiscale Investigation of Oxidative Aging in Biomodified Asphalt Binder. *The Journal of Physical Chemistry*. https://doi.org/10.1021/acs.jpcc.6b05004

Navarro, F. J., Partal, P., García-Morales, M., Martinez-Boza, F. J., & Gallegos, C. (2007). Bitumen modification with a low-molecular-weight reactive isocyanate-terminated polymer. *Fuel*, *86*(15), 2291–2299. https://doi.org/10.1016/j.fuel.2007.01.023

Nellensteyn, F. J., & Roodenburg, N. M. (1933). Die Ausbreitung von Wasser auf Asphaltbitumen und Teer. *Kolloid-Zeitschrift*, *63*(3), 339–347. https://doi.org/10.1007/BF01422945

Oliviero Rossi, C., Spadafora, A., Teltayev, B., Izmailova, G., Amerbayev, Y., & Bortolotti, V. (2015). Polymer modified bitumen: Rheological properties and structural characterization. *Colloids and Surfaces A: Physicochemical and Engineering Aspects*, *480*, 390–397. https://doi.org/10.1016/J.COLSURFA.2015.02.048

Pauli, A. T., Grimes, R. W., Beemer, A. G., Turner, T. F., & Branthaver, J. F. (2011). Morphology of asphalts, asphalt fractions and model wax-doped asphalts studied by atomic force microscopy. *International Journal of Pavement Engineering*, *12*(4), 291–309. https://doi.org/Doi

10.1080/10298436.2011.575942

Pfeiffer, J. P., & Saal, R. N. J. (1940). Asphaltic Bitumen as Colloid System. *The Journal of Physical Chemistry*, *44*(2), 139–149. https://doi.org/10.1021/j150398a001

Rashid, F., Hossain, Z., & Bhasin, A. (2019). Nanomechanistic properties of reclaimed asphalt pavement modified asphalt binders using an atomic force microscope. *International Journal of Pavement Engineering*, *20*(3), 357–365. https://doi.org/10.1080/10298436.2017.1293268

Schindelin, J., Arganda-Carreras, I., Frise, E., Kaynig, V., Longair, M., Pietzsch, T., … Cardona, A. (2012). Fiji: an open-source platform for biological-image analysis. *Nature Methods*, *9*(7), 676–682. https://doi.org/10.1038/nmeth.2019

Soenen, H., Besamusca, J., Fischer, H. R., Poulikakos, L. D., Planche, J.-P., Das, P. K., … Chailleux, E. (2014). Laboratory investigation of bitumen based on round robin DSC and AFM tests. *Materials and Structures*, *47*(7), 1205–1220. https://doi.org/10.1617/s11527-013-0123-4